The Swift-XRT (Gehrels et al. 2004; Burrows et al. 2005) is an X-ray telescope with an effective area peaking at 110 cm^2 at 1.5 keV, it has a 23.6×23.6 arc min field of view, and an energy bandpass of 0.3–10 keV. The vicinity of the January trigger was observed by Swift in 5 overlapping fields (Fig. 1). Each of these were observed twice that month. For the September trigger two disjoint Swift fields were observed (Fig. 1). Each being observed twice, once in 2010 September and again 2010 December. Details of the observations are given in Tables 1– 2.

We analysed the Swift-XRT data with custom scripts which use the software developed by Evans et al. (2007, 2009). For each field we combined the observations and produced a single image and exposure map. We then used the source detection and PSF fitting code described in Goad et al. (2007) and Evans et al. (2009) to identify and localise sources in the field. This method uses a sliding-cell detection algorithm, with a fixed cell size of 21×21 pixels (which encloses 93% of the PSF). An initial run with a detection significance threshold of 3 (i.e. the counts in the cell should be at least $B+3\sqrt{B}$ where B is the number of background counts expected in the cell, measured from an annular box of size 51 pixels) revealed no sources in any of the observations. However, for faint sources this box size is sub-optimal. We therefore performed a second pass, lowering the detection threshold to 1.5. We measured the mean background level in each field and, using a circular source region of radius $23.6''$ centred on each source we applied the Bayesian test of Kraft, Burrows & Nousek (1991) which confirmed that all of these sources were detected with at least 99.7% confidence (i.e. 3 σ detections): the source positions are given in Tables 3–4.

Each of these reduced-threshold detections has very few photons, therefore it was not useful to perform a detailed spectral or temporal analysis. We determined the mean count-rate of each detection using the Bayesian method of Kraft et al. (1991) and then applied corrections of PSF losses and instrumental affects, following the processes described by Evans et al. (2007, 2009). We used PIMMS[1] to determine a count rate-to-flux conversion factor. Assuming a power-law spectrum with a photon index of 1.7, and an absorbing column of 3×10^{21} cm^{-2} (the Galactic value in the direction of the LIGO trigger, Kalberla et al. 2005), we find a 0.3-10 keV conversion factor of 5.1×10^{-11} erg cm^{-2} ct^{-1}.

Given the sky area covered by the Swift observations (0.15 square degrees per field) we expect to find a number of serendipitous sources in the XRT data. To quantify the likelihood that each detected X-ray source is serendipitous, we used the 2XMMi-DR3 catalogue (Watson et al. 2008 A&A 493,339). We selected from this catalogue all unique good sources (i.e. with a quality flag of 0). For consistency with 2XMMi-DR3 we convert the 0.3–10 keV XRT count-rates into 0.2–12 keV fluxes, using an absorbed power-law spectrum with a column of $N_{\mathrm{H}} = 3 \times 10^{20}$ cm^{-2} and a power-law photon index $\Gamma = 1.7$, as used for 2XMM[2], and then counted the number of 2XMMi-DR3 sources with M1_8_FLUX values (i.e. 0.2–12 keV MOS-1 flux) at least as bright as the XRT

[1] http://heasarc.gsfc.nasa.gov/cgi-bin/Tools/w3pimms/pim
[2] http://xmmssc-www.star.le.ac.uk/Catalogue/2XMM/UserGuide_xmmcat.html#TabECFs

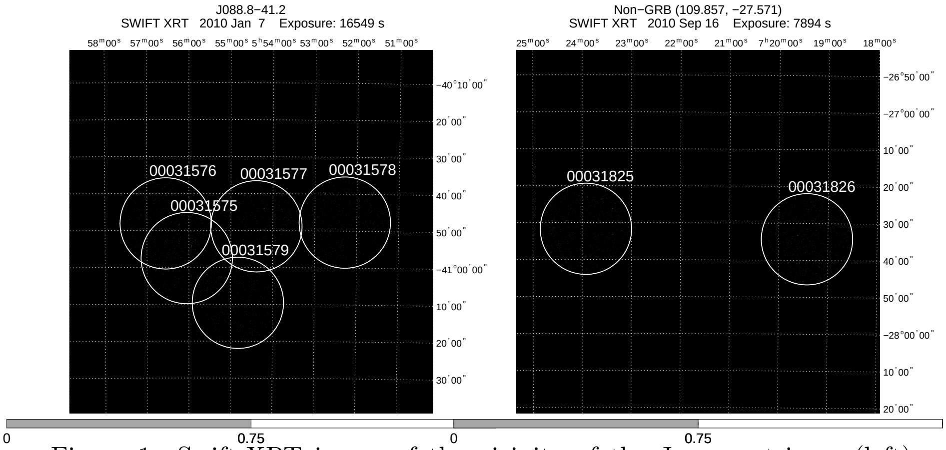

Figure 1: Swift-XRT image of the vicinity of the January trigger (left) and February trigger (right). The large circles show the fields of view of the various pointings.

source. This was then scaled by the ratio of the Swift-XRT instantaneous field of view (0.35 square degrees) to the 2XMMi-DR3 unique sky coverage area (504 square degrees). This yielded, for each Swift source, the number of serendipitous sources of that brightness expected in a single Swift field of view. These values, along with the mean brightnesses, are given in Tables 5–6. This analysis did not account for any inhomogeneities in the spatial distribution of sources in the 2XMM catalogue.

We also performed a variability test, since an EM counterpart to the LIGO trigger may be expected to be fading. To do this we produced a light curve of each source, creating one bin per obsID[3], and determining the count-rate using the Bayesian method (Kraft et al. 1991). The significance of any variability was then found simply by dividing the difference in the two bins by the errors in the two bins, added in quadrature. This is given in Tables 5–6; two sources show moderate evidence for variability (January Source #1 and September Source #6).

[3]For the September trigger we excluded the second observation of each source, since this was very short

Table 1: Details of the Swift-XRT follow-up observations of the January trigger.

ObsID	Date Start (UT)	Date End (UT)	Exposure) (ks)	Pointing Direction J2000
00031575001	2010 Jan 07 at 13:04	2011 Jan 07 at 14:29	1.5	89.07°, -40.96°
00031575002	2010 Jan 11 at 19:11	2010 Jan 11 at 19:38	1.6	89.00°, -40.92°
00031576001	2010 Jan 07 at 14:33	2010 Jan 07 at 15:55	1.7	89.14°, -40.80°
00031576002	2010 Jan 11 at 15:59	2010 Jan 11 at 16:18	1.1	89.13°, -40.77°
00031577001	2010 Jan 07 at 15:57	2010 Jan 07 at 17:20	1.8	88.60°, -40.81°
00031577002	2010 Jan 11 at 17:35	2010 Jan 11 at 18:02	1.6	88.60°, -40.76°
00031578001	2010 Jan 07 at 17:23	2010 Jan 07 at 18:49	2.0	88.07°, -40.79°
00031578002	2010 Jan 11 at 13:18	2010 Jan 11 at 15:01	1.4	88.06°, -40.78°
00031579001	2010 Jan 07 at 20:26	2010 Jan 07 at 20:59	2.0	88.71°, -41.16°
00031579002	2010 Jan 11 at 18:03	2010 Jan 11 at 19:51	1.4	88.77°, -41.17°

Table 2: Details of the Swift-XRT follow-up observations of the 2010 September trigger.

ObsID	Date Start (UT)	Date End (UT)	Exposure) (ks)	Pointing Direction J2000
00031825001	2010 Sep 16 at 18:10	2010 Sep 16 at 18:35	1.5	110.98°, -27.53°
00031825002	2010 Dec 30 at 03:17	2010 Dec 30 at 03:19	0.09	110.98°, -27.54°
00031825003	2010 Dec 30 at 00:06	2010 Dec 30 at 03:34	2.3	110.98°, -27.53°
00031826001	2010 Sep 16 at 19 36	2010 Sep 16 at 20:09	2.0	109.86°, -27.57°
00031826002	2010 Dec 29 at 03:37	2010 Dec 29 at 04:50	0.14	109.85°, -27.54°
00031826003	2010 Dec 29 at 03:38	2010 Dec 29 at 05:09	1.9	109.86°, -27.58°

Table 3: The reduced-threshold sources detected in the X-ray data for the January event.

Source #	RA (J2000)	Dec (J2000)	Error ($''$ 90 conf.)
1	05h 55m 1.00s	-40°58′ 00.8″	4.5
2	05h 57m 4.80s	-40°54′ 45.4″	4.3
3	05h 54m 12.72s	-40°44′ 05.8″	4.3
4	05h 54m 59.29s	-40°54′ 19.6″	4.5
5	05h 51m 57.66s	-40°46′ 10.9″	5.6
6	05h 51m 41.12s	-40°44′ 46.4″	5.5
7	05h 52m 6.29s	-40°59′ 14.3″	6.5
8	05h 52m 55.88s	-40°46′ 14.9″	5.2

Table 4: The reduced-threshold sources detected in the X-ray data for the September event.

Source #	RA (J2000)	Dec (J2000)	Error ($''$ 90 conf.)
1	07h 23m 22.99s	-27°26′ 10.1″	4.4
2	07h 23m 22.34s	-27°33′ 09.5″	4.4
3	07h 23m 34.43s	-27°23′ 32.4″	5.4
4	07h 24m 34.95s	-27°31′ 31.1″	6.1
5	07h 23m 53.50s	-27°23′ 06.5″	4.4
6	07h 24m 27.89s	-27°35′ 40.8″	6.5
7	07h 23m 54.14s	-27°42′ 29.5″	6.4
8	07h 19m 30.22s	-27°45′ 42.5″	4.1
9	07h 19m 37.14s	-27°33′ 12.0″	5.2
10	07h 19m 25.72s	-27°31′ 37.0″	5.8
11	07h 19m 18.04s	-27°25′ 15.4″	5.0
12	07h 19m 41.92s	-27°39′ 58.1″	5.0

Table 5: Details of the X-ray sources detected in the follow-up observations of the January trigger.
[1] N_s is the number of 2XMMi-DR3 sources which are at least as bright as the Swift source, which are expected in a single Swift field. See text for details

Source #	Count Rate (0.3–10 keV, ks^{-1})	N_s^1	Variability significance (σ)
1	$5.9^{+1.5}_{-1.2}$	0.9	2.05
2	$5.9^{+2.1}_{-1.6}$	0.9	0.26
3	$4.6^{+1.5}_{-1.2}$	1.3	0.45
4	$3.2^{+1.3}_{-1.0}$	2.4	0.75
5	$2.8^{+1.8}_{-1.1}$	2.9	1.10
6	$1.4^{+1.1}_{-0.7}$	7.5	0.74
7	$2.3^{+1.2}_{-0.8}$	3.9	0.91
8	$2.9^{+1.7}_{-1.2}$	2.8	0.00

Table 6: As Table 5 but for the September trigger.

Source #	Count Rate (0.3–10 keV, ks^{-1})	N_s^1	Variability significance (σ)
1	$2.8^{+0.9}_{-0.7}$	2.9	1.47
2	$2.3^{+1.1}_{-0.7}$	3.9	1.09
3	$2.4^{+1.1}_{-0.8}$	3.7	1.47
4	$1.8^{+1.2}_{-0.7}$	5.5	1.01
5	$0.6^{+0.3}_{-0.2}$	17	1.30
6	$2.3^{+1.1}_{-0.7}$	3.9	2.48
7	$2.2^{+1.0}_{-0.7}$	4.2	1.20
8	$8.8^{+3.4}_{-2.4}$	0.5	0.44
9	$2.4^{+1.1}_{-0.8}$	3.7	0.60
10	$0.9^{+0.6}_{-0.3}$	12	0.36
11	$1.7^{+0.9}_{-0.6}$	5.9	0.97
12	$1.6^{+1.2}_{-0.7}$	6.4	1.02